DOI:10.1190/segam2021-3583664.1

Mapping the salt structures from magnetic and gravity gradiometry data in Nordkapp Basin, Barents Sea

Mo Tao, Michael Jorgensen, and Michael S. Zhdanov, Consortium for Electromagnetic Modeling and Inversion, University of Utah, and TechnoImaging*

Summary

Accurate interpretation of salt structures plays an important role in hydrocarbon exploration. Over the years, several methods have been applied to mapping salt structures, including seismic, gravity and magnetic. The gravity and magnetic methods in particular have the advantages of low cost, efficiency, and ability to map the salt flanks and base of the salt, which are critical in oil and gas exploration. The salt diapirs are characterized by diamagnetic properties which makes a standard magnetic inversion for susceptibility difficult to apply. In this paper, we apply a recently developed method of total magnetic intensity (TMI) data inversion for magnetization vector instead of susceptibility. The magnetization vector can change its orientation within the inversion domain, thus indicating different types of magnetic properties of the rocks. The 3D inversion for magnetization vector, however, becomes very complicated due to the increased non-uniqueness of the inverse problem. To address this ambiguity, we use a joint inversion of gradiometry and TMI data based on a joint focusing stabilizer. This novel approach is illustrated by the case study of mapping the sea-bottom salt structures in the Nordkapp Basin of Barents Sea.

Introduction

Salt domes and salt diapirs represent important targets in offshore hydrocarbon (HC) exploration because oil and gas deposits are often associated with these structures. The traditional approach to offshore oil and gas exploration is based on seismic methods. Interpretation of seismic data in the presence of salt formations; however, could be a very challenging problem, due to the large contrast of acoustic impedance between the salt and surrounding host rocks (Hokstad et al., 2011; Paoletti et al. 2020). Compared to the seismic method, gravity (gradiometry) and magnetic data can provide better defined salt boundaries, especially of the salt flanks and salt base (e.g., Fichler et al.2007; Gernigon et al. 2011; Stadtler et al. 2014; Paoletti et al. 2020). The salt structures are usually characterized by low density and diamagnetic properties compared to the surrounding rocks (Gernigon et al., 2011). Several successful case studies using seismic and gravity (gradiometry) data for mapping the salt structures for offshore exploration have been published (e.g., Wan and Zhdanov, 2008; Tu and Zhdanov, 2020; Xu et al., 2020). However, only a few papers have been published on application of magnetic field data for salt imaging (e.g., Bain et al., 1993; Paoletti et al., 2020).

In some areas, it can be challenging to obtain a geologically meaningful inverse magnetic susceptibility model while honoring the data. This problem could be caused by the presence of remanent magnetization or diamagnetic materials. This problem can be addressed by inverting for magnetization vector as opposed to magnetic susceptibility only (Lelièvre and Oldenburg, 2009; Li et al., 2010; Ellis et al., 2012; Zhu et al., 2015; Li, 2017). Inversion for magnetization vector introduces more degrees of freedom into the inversion process, which increases non-uniqueness. We remedy this problem of non-uniqueness by inverting total magnetic intensity (TMI) data jointly with gravity gradiometry data. The case study presents the results of joint inversion of the marine full tensor gravity gradiometry (FTG) data and airborne TMI data collected over the Nordkapp Basin, Barent Sea.

Theory

In general, the inverse problem can be expressed as the following equation:

$$d = A(m), \quad (1)$$

Our goal is to determine the model m based on known forward operator, A, and observed data d. This is usually an ill-posed problem, which requires regularization. We apply minimization of the Tikhonov parametric functional:

$$P^{\alpha}(m) = \varphi(m) + \alpha s(m) = min, \quad (2)$$

where $\varphi(m)$ is misfit functional; $s(m)$ is stabilizing functional; and α is regularization parameter

In a case of jointly inverting two datasets, gravity and magnetic, we select the following specific form of the parametric functional with the joint focusing stabilizer, $s_{jf}(m^{(1)}, m^{(2)})$:

$$P = \sum_{i=1}^{2} \varphi\left(m^{(i)}\right) + \alpha s_{jf}\left(m^{(1)}, m^{(2)}\right), \quad (3)$$

where $m^{(1)} = \rho$ is the density model, and $m^{(2)} = \{M_x, M_y, M_z\}$ is the magnetization vector model. We invert for all components of the magnetization vector; however, it is important to note that only vertical (Z) component of the magnetization vector is included in the focusing stabilizer. Future work will include incorporation of all components in the stabilizer. This approach is justified by the results of standalone magnetization vector inversion, where the vertical component of magnetization vector is dominant, which is the case in Nordkapp Basin. Thus, the focusing term incorporates the density and the vertical (Z) component of the magnetization vector to reduce non-uniqueness, as follows:

$$s_{jf}\left(m^{(1)}, m^{(2)}\right) =$$

$$\iiint_V \frac{\sum_{i=1}^{2} W_{m,j}^{(i=1(2))} (m_{(z)}^{(i=1(2))} - m_{(z)apr}^{(i=1(2))})^2}{\sum_{i=1}^{2} W_{m,j}^{(i=2(1))} (m_z^{(i=2(1))} - m_{z,apr}^{(i=2(1))})^2 + e^2} dv, \quad (4)$$

where $m^{(1)} = \rho$ is the density model; $m_z^{(2)} = M_z$ is the vertical component of the magnetization vector; and coefficient e is the focusing parameter (Zhdanov, 2015; Molodtsov and Troyan, 2017). The joint minimum support constraint is not enforced until the data misfit corresponding to both models reaches the level $\chi^2 = 2$, to avoid the introduction of spurious features in the joint focusing inversion (Jorgensen and Zhdanov, 2020).

It is important also having an additional level of data and model weighting to ensure a similar scale of both geophysical data sets in the joint inversion. In this project, the observed data are weighted by the related errors:

$$W_d^{(i)} = \frac{1}{\left(e_f^{(i)} d^{(i)} + e_{abs}^{(i)}\right)}, \quad (5)$$

where $e_f^{(i)}$ are the relative errors and $e_{abs}^{(i)}$ are the absolute errors. In the joint inversions, data weights are further scaled by the initial data misfit for each data set:

$$W_{d,j}^{(i)} = \frac{W_d^{(i)}}{\varphi_{ini}(m^{(i)})}, \quad (6)$$

where $\varphi_{ini}\left(m^{(i)}\right)$ are the initial misfits.

The model weights for density are determined by integrated sensitivity (Zhdanov, 2015):

$$W_m^{(i1)} = diag \sqrt[4]{F^{(i)T} F^{(i)}}, \quad (7)$$

where $F^{(i)}$ is Fréchet derivative of the corresponding forward operator, $A^i(m^i)$; $F^{(i)T}$ is the transposed Fréchet.

In the joint inversions, the model weights for density are further scaled as follows:

$$W_{m,j}^{(1)} = \frac{W_m^{(1)}}{max(m_{sep}^{(1)} - m_b^{(1)})}, \quad (8)$$

where $m_{sep}^{(1)}$ are the models obtained from standalone inversion; $m_b^{(1)}$ is a background model.

In the same way, the model weights for the magnetization vector are determined as follows:

$$W_{m_\gamma}^{(2)} = \left\{ diag \sqrt[4]{F_\gamma^{(2)T} F_\gamma^{(2)}} \right\}, (\gamma = x, y, z), \quad (9)$$

and in the joint inversion the model weights are further scaled as follows:

$$W_{m,j}^{(2)} = \left\{ \frac{W_{m\gamma}^{(2)}}{max\left(m_{sep_\gamma}^{(2)} - m_{b_\gamma}^{(2)}\right)} \right\}, (\gamma = x, y, z), \quad (10)$$

Case study

The Nordkapp Basin (NKB), located in the southwestern Barent Sea, is about 300 km long and 30-80 km wide, and it has a narrow graben-type structure. Our study area is selected in the southern sub-basin of the NKB (Figure 1). A marine full tensor gravity gradiometry (FTG) survey has been conducted by Bell Geospace on behalf of StatoilHydro in 2008. Also, recently the high-resolution aeromagnetic data were acquired by the Geological Survey of Norway. The height of the cesium magnetometer was set at ~230 m above sea level, and the line spacing was 500 m. Most of the diapirs are located near the seabed, and the average depth of the sea is about 300 m.

The expectations are that FTG anomalies could help to map the geometries of salt diapirs in Nordkapp basin. Indeed, the density range of the host rocks in the study area is approximately 2.30—2.38 g⁄cc, and the salt diapirs are characterized by density anomalies with negative values around -0.2— -0.4 g⁄cc (Xu et al., 2020). At the same time, these salt diapers are diamagnetic and have a negative magnetization contrast with respect to the surrounding Tertiary sea-bottom formations.

The gravity gradiometry and TMI data were filtered to eliminate the responses from the deeper sources by using regional trend removal. The inversion domain was discretized by rectangular cells with $325 \times 325 m^2$ horizontal size and vertical size logarithmically increasing with the total depth to 3400 m. The total grid size was ~60,071 cells. The horizontal size of inversion area was $20 \times 10\ km^2$.

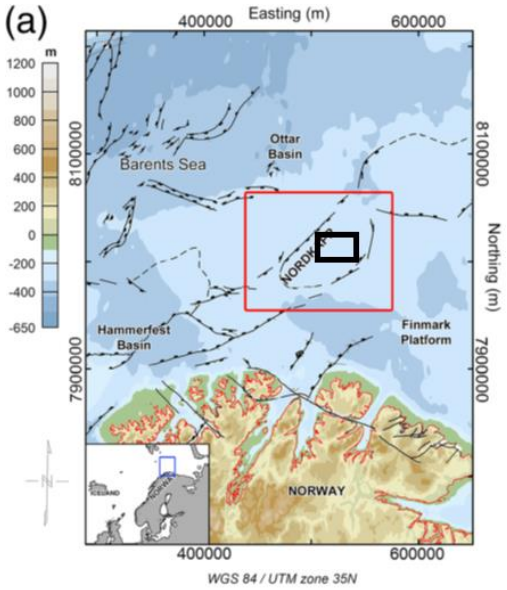

Figure 1: Map of Nordkapp basin, Barent sea (after Paoletti et al. 2020), the red square includes area of FTG and high resolution aeromagnetic survey. The black box shows the inversion area.

Figure 2 presents a map of the observed TMI data showing the inversion area. The red dot lines indicate the location of profiles AA', BB' and CC', which will be analyzed in the next section.

Results

Figure 3 shows, as an example, a comparison between the observed and predicted Gzz and TMI data produced by standalone and joint focusing inversions. We can see that the observed data fit predicted data very well.

Figure 4 presents the vertical sections of inversion results along profiles AA', BB' and CC', shown in Figure 2. The standalone inversion results contrast the joint inversion results shown in Figures 4, 5, and 6. From these results, we can see that the joint focusing inversion helped to "clean up" the distortions of the inverse images in the deep areas. The produced images of the density and magnetization models become clearer and with sharper boundaries.

We should note that, the white arrows in these figures represent the direction and strength of magnetization vector produced by the inversion; the red bold arrow indicates the direction of inducing magnetic field. It is interesting to note that, the magnetization vectors within the salt diapirs point upward at the direction opposite to the direction of the inducing magnetic field (shown by bold red arrow), which indicates a diamagnetic property of the salt structures. At the same time, the magnetization vector changes its direction outside the diapirs and points downward in the direction of the inducing magnetic field, which is typical for paramagnetic minerals present in Cretaceous sea-bottom layers of the host formations (Paoletti et al., 2020). The spatial distribution of the magnetization vector, produced by the joint inversion, could serve as a good indicator of the geometry of the salt diapirs in the Nordkapp basin.

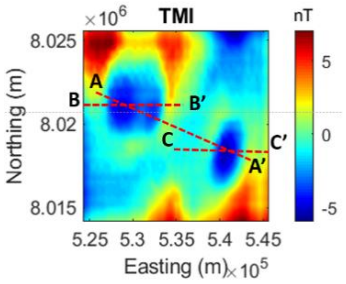

Figure 2: This is the observed TMI data map showing the inversion area. Red dot lines showed the location of profile AA', BB' and CC'.

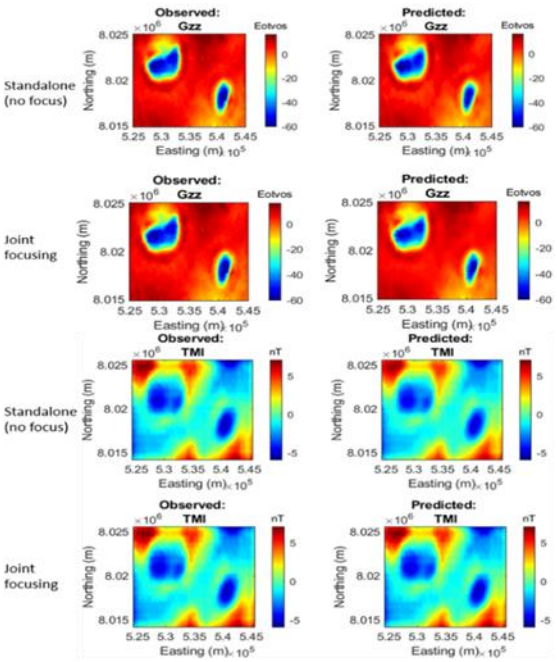

Figure 3. Upper panels show the observed and predicted Gzz component of gravity gradient field data from standalone and joint inversions, respectively. Lower panels present the observed and predicted TMI data from standalone and joint focusing inversions, respectively.

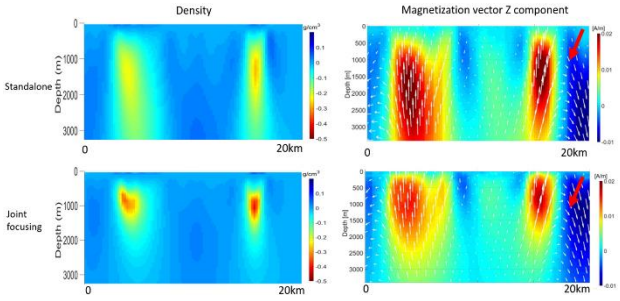

Figure 4. Profile AA': Vertical sections of the density and magnetization models produced by standalone and joint focusing inversions, respectively. The white arrows represent the magnetization vector; the red bold arrow indicates the direction of inducing field. The color bars show density and Mz, respectively.

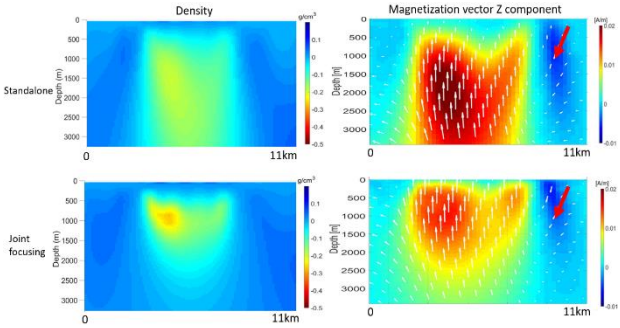

Figure 5. Profile line BB': Vertical sections of the density and magnetization models produced by standalone and joint focusing inversions, respectively. The white arrows represent the magnetization vector; the red bold arrow indicates the direction of inducing field. The color bars show density and Mz, respectively.

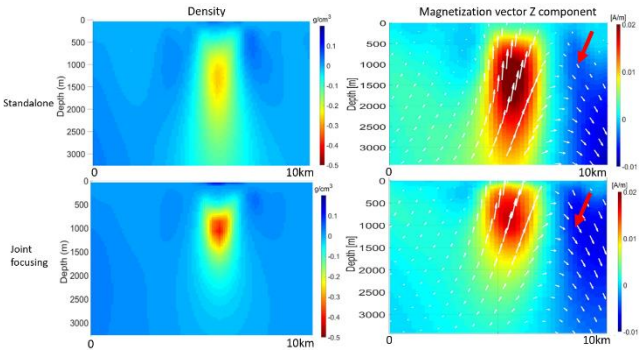

Figure 6. Profile line CC': Vertical sections of the density and magnetization models produced by standalone and joint focusing inversions, respectively. The white arrows represent the magnetization vector; the red bold arrow indicates the direction of inducing field. The color bars show density and Mz component, respectively.

Conclusions

We consider a novel approach to the inversion of the TMI data for magnetization vector based on joint analysis of magnetic and gravity gradiometry data. By jointly inverting two different data sets, we improve the robustness and reduce the ambiguity of the potential field inversions.

This approach was used for jointly inverting marine gravity gradiometry and airborne TMI data collected over the Nordkapp Basin, Barents Sea. These data types were chosen for Nordkapp basin because the main geological targets in this area, the salt diapirs, are characterized by low density and diamagnetic anomaly compared to the surrounding sea-bottom layers. The results of inversion demonstrate that the position and geometry of the salt diapirs can be clearly seen in the density and magnetization inverse models. Remarkably, we can also observe a change of magnetization vector directions from diamagnetic diapirs to surrounding sea-bottom paramagnetic rocks.

Our results are also in a good agreement with the published results of the standalone gravity gradiometry and magnetic data inversions for the same area (Xu et al., 2020; Paoletti et al., 2020)

Acknowledgments

The authors acknowledge Consortium for Electromagnetic Modeling and Inversion (CEMI) at the University of Utah and TechnoImaging for the support of this research. The FTG data were collected by Bell Geospace on behalf of StatoilHydro and the high resolution aeromagnetic data were acquired by the Geological Survey of Norway. We are thankful to Dr. B. Farrelly for providing the data.

REFERENCES

Bain, J., T. R. Horscroft, J. Weyand, A. H. Saad, and D. N. Bulling, 1993, Complex salt features resolved by integrating seismic, gravity and magnetics: 55th Conference and Technical Exhibition, European Association of Petroleum Geophysicists (EAGP)/European Association of Exploration Geophysicists (EAEG), 1–4, doi: https://doi.org/10.3997/22144609.201411696.

Ellis, R. G., B. De Wet, and I. N. Macleod, 2012, Inversion of magnetic data from remanent and induced sources: Proceedings of the 22nd ASEG Geophysical Conference and Exhibition, Expanded Abstracts.

Fichler, C., H. Rueslåtten, C. Gram, A. Ingebrigtsen, and O. Olesen, 2007, Salt interpretation with special focus on magnetic data, Nordkapp Basin, Barents Sea: 2007 International workshop Innovation in EM, Grav and Mag Methods (EGM 2007): A New Perspective for Exploration, Extended Abstract.

Gernigon, L., M. Bronner, C. Fichler, L. Lovas, L. Marello, and O. Olesen, 2011, Magnetic expression of salt diapir marinerelated structures in the Nordkapp Basin, western Barents Sea: Geology, **39**, 135–138, doi: https://doi.org/10.1130/G31431.1.

Hokstad, K., B. Fotland, G. Mackenzie, V. Antonsdottir, S.-K. Foss, C. Stadtler, C. Fichler, M. Haverl, B. M. T. Waagan, E. A. Myrlund, L. Masnaghetti, F. Ceci, and P.-Y. Raya, 2011, Joint imaging of geophysical data: Case history from the Nordkapp Basin, Barents Sea: SEG Technical Program, Expanded Abstracts, 1098–1102, doi: https://doi.org/10.1190/1.3627395.

Jorgensen, M., and M. S. Zhdanov, 2020, 3D joint inversion of potential field data in the presence of remanent magnetization: 90th Annual International Meeting, SEG, Expanded Abstracts, 1949–4645, doi: https://doi.org/10.1190/segam2020-3427184.1.

Lelièvre, P. G., and D. W. A. Oldenburg, 2009, 3D total magnetization inversion applicable when significant, complicated remanence is present: Geophysics, **74**, no. 3, L21–L30, doi: https://doi.org/10.1190/1.3103249.

Li, Y., 2017, From susceptibility to magnetization: Advances in the 3D inversion of magnetic data in the presence of significant remanent magnetization: Proceedings of the Exploration 17: Sixth Decennial International Conference on Mineral Exploration, 239–260.

Li, Y., S. E. Shearer, M. M. Haney, and N. Dannemiller, 2010, Comprehensive approaches to 3D inversion of magnetic data affected by remanent magnetization: Geophysics, **75**, no. 1, L1–L11, doi: https://doi.org/10.1190/1.3294766.

Molodtsov, D., and V. Troyan, 2017, Multiphysics joint inversion through joint sparsity regularization: 87th Annual International Meeting, SEG, Expanded Abstracts, 1262–1267, doi: https://doi.org/10.1190/segam2017-17792589.1.

Paoletti, V., M. Milano, J. Baniamerian, and M. Fedi, 2020, Magnetic field imaging of salt structures at Nordkapp Basin, Barents Sea: Geophysical Research Letters, **47**, e2020GL089026, doi: https://doi.org/10.1029/2020GL089026.

Stadtler, C., C. Fichler, K. Hokstad, E. A. Myrlund, S. Wienecke, and B. Fotland, 2014, Improved salt imaging in a basin context by high resolution potential field data: Nordkapp Basin, Barents Sea: Geophysical Prospecting, **62**, 615–630, doi: https://doi.org/10.1111/1365-2478.12101.

Tu, X., and M. Zhdanov, 2020, Enhancement and sharpening the migration images of the gravity field and its gradients: Pure and Applied Geophysics, **177**, 2853–2870, doi: https://doi.org/10.1007/s00024-019-02397-9.

Wan, L., and M. S. Zhdanov, 2008, Focusing inversion of marine full tensor gradiometry data in offshore geophysical exploration: 78th SEG Technical Program, Expanded Abstracts, 751–754, doi: https://doi.org/10.1190/1.3063755.

Xu, Z., L. Wan, and M. Zhdanov, 2020, Focusing iterative migration of gravity gradiometry data acquired in Nordkapp basin, Barents Sea: Geophysical Prospecting, **68**, 2292–2306, doi: https://doi.org/10.1111/1365-2478.12990.

Zhdanov, M. S., 2009, Geophysical electromagnetic theory and methods: Elsevier.

Zhdanov, M. S., 2015, Inverse theory and applications in geophysics: Elsevier.

Zhdanov, M. S., and M. Cuma, 2018, Joint inversion of multimodal data using focusing stabilizers and Gramian constraints: 88th Annual International Meeting, SEG, Expanded Abstracts, 1430–1434, doi: https://doi.org/10.1190/segam2018-2998495.1.

Zhu, Y., M. S. Zhdanov, and M. Cuma, 2015, Inversion of TMI data for the magnetization vector using Gramian constraints: Proceedings of the 85th SEG International Exposition and Annual Meeting, Expanded Abstracts, 1602–1606, doi: https://doi.org/10.1190/segam2015-5855046.1.